



LETTER

Ferromagnetism evidence and size dependence in ferroelectric PZN-4.5PT nanoparticles

To cite this article: Rémi Ndioukane *et al* 2019 *EPL* **125** 47004

View the [article online](#) for updates and enhancements.

Ferromagnetism evidence and size dependence in ferroelectric PZN-4.5PT nanoparticles

RÉMI NDIUKANE^{1(a)}, MOUSSA TOURÉ¹, DIOUMA KOBOR^{1(b)}, YOANN LALATONNE², LAURENCE MOTTE², LAURENT LEBRUN³, MARIN TADIC⁴ and FABRICE WILHELM⁵

¹ *Laboratoire de Chimie et de Physique des Matériaux (LCPM), University, Assane Seck of Ziguinchor (UASZ) Quartier Néma 2, BP 523, Ziguinchor, Senegal*

² *Inserm, U1148, Laboratory for Vascular Translational Science, Université Paris 13, Sorbonne Paris Cité F-93017 Bobigny, France*

³ *Univ Lyon, INSA-Lyon, LGEF, EA682 - 8 rue de la Physique, F-69621, Villeurbanne, France*

⁴ *Institute for Nuclear Sciences Vinca, University of Belgrade - Mike Petrovica Alasa 12-14 POB 522, 11351 Vinca, Belgrade, Serbia*

⁵ *ESRF - 71 Avenue des Martyrs, F-38000 Grenoble, France*

received 8 November 2018; accepted in final form 14 February 2019

published online 22 March 2019

PACS 75.75.-c – Magnetic properties of nanostructures

PACS 77.55.Nv – Multiferroic/magnetolectric films

PACS 77.80.-e – Ferroelectricity and antiferroelectricity

Abstract – In this work we show the size-dependent ferromagnetic behavior of undoped and Mn-doped PZN-4.5PT single crystals, consequently their multiferroic one. Undoped single crystals were tamized and three different sizes powders were investigated showing a size dependence in such ferroelectric materials while no magnetism is observed for the non-oriented and oriented bulk single crystals. The results show the existence of an optimized grain sizes range ($45 \mu\text{m} \leq D \leq 63 \mu\text{m}$) in which the magnetism is the highest (around 0.08 emu/g). It is found that the maximum value of the relative strain decreases from 0.25% for undoped crystals to 0.20% for Mn-doped ones. The remanent magnetization M_r and coercivity (H_c) were found equal, respectively, to 2×10^{-4} emu/g and 63 Oe for undoped and, 7×10^{-4} emu/g and 66 Oe for Mn-doped PZN-4.5PT, indicating that PZN-4.5PT particles possessed weak ferromagnetic behavior. Mn doping increases highly the spontaneous magnetization from 7.5×10^{-3} emu/g to 1.0×10^{-3} emu/g, respectively for undoped and Mn-doped nanoparticles.

Copyright © EPLA, 2019

Introduction. – Among various everlasting desires of materials scientists, the most important is the research of materials with the best possible functionalities [1,2]. Transition metals have a very rich chemistry due to a variable oxidation state, which offers a multitude of interesting properties, if selected judiciously. Numerous metal oxides have been investigated and are being studied for various technological applications [3–6]. To overcome the scarcity of single-phase multiferroics, various approaches have been used to artificially synthesize new multiferroic materials. With a steadily increasing interest to fabricate multiferroics, PbTiO_3 is being extensively looked into for composites of ferroelectric and ferromagnetic heterostructures,

super-lattices composed of alternating ferroelectric and ferromagnetic layers and doping of suitable magnetic transition metals [7–10].

However, it has been reported in the literature that the reactivity and structural non-compatibility between the two materials or with the substrate generate difficulties in fabricating heterostructures and achieving coupling between the two order parameters.

Therefore, research has mainly focused on inducing magnetoelectric effects in the ferroelectric materials by suitable doping (Fe, Mn, Ni, etc.). Ferroelectric single crystals $\text{Pb}(\text{Zn}_{1/3}\text{Nb}_{2/3})\text{O}_3$ - PbTiO_3 (PZN-PT) may be promising full materials for such devices. Indeed, during the past few years, published results have pointed at high levels of piezoelectricity in $\text{Pb}(\text{Mg}_{1/3}\text{Nb}_{2/3})\text{O}_3$ - PbTiO_3 (PMN-PT) and PZN-PT single crystals [11–14],

^(a)E-mail: remindiukane@gmail.com

^(b)Corresponding author

showing at least ferroelectric, ferroelastic and piezoelectric properties. However, the greatest difficulty in using such single crystals on electronic devices is to achieve them in thin layers form because of their incongruent melting property.

This paper describes ferroelectric 99.5Pb(Zn_{1/3}Nb_{2/3})O₃-4.5PbTiO₃ (PZN-4.5PT) single crystals, synthesized by the flux method [12]. After having been ground into nanopowders, the undoped and Mn-doped PZN-4.5PT particles as well as bulk and oriented single crystals structural, ferroelectric and ferromagnetic properties were investigated.

Experimental procedure. – Undoped and 1% Mn-doped PZN-4.5PT single crystals that had been synthesized by the flux method [12] were ground in a mortar to obtain a very fine nanopowder. To exclude contamination, grounding process was repeated in two different laboratories (in LVST, Paris 13, France and in LCPM, UASZ, Ziguinchor, Senegal, with different types of mortars fabricated with different chemical components (free-ferromagnetic elements: SiC (in LCPM, Senegal) and WC (in LVST, Paris, France)). The as-synthesized powders were characterized by TEM analysis using a FEI CM10 microscope (Philips) by depositing a drop of nanoparticles suspension on carbon coated copper grids placed on a filter paper. Ferroelectric characterization was carried out on $1 \times 1 \times 0.1 \text{ cm}^3$ flat samples with two parallel faces sputtered with gold and oriented $\langle 110 \rangle$. Poling was performed with an electric field of 12 kV/cm at room temperature. A modified Sawyer-Tower circuit at room temperature was used to measure the polarization *vs.* the DC field. From polarization- E_{field} curves, coercive field (E_c), remanant polarization (P_r) and spontaneous polarization (P_s) were determined. The magnetic hysteresis loops were measured using a vibrating sample magnetometer (VSM) model Quantum Design Versalab for bulk, oriented bulk and nanoparticles for size effect. The results made possible to determine the saturation and remnant magnetization and coercivity.

Results and discussion. – Figure 1 presents TEM micrographs of the PZN-4.5PT (fig. 1(a) and fig. 1(b)) and PZN-4.5PT+1% Mn (fig. 1(c) and fig. 1(d)) nanoparticles. According to these images, the undoped crystals consisted mainly of spherical nanoparticles with a diameter between 30 and 100 nm, whereas the doped ones were made up of both spherical nanoparticles with diameters ranging from 30 to 100 nm (fig. 1(c)) and nanosticks with lengths up to 200 nm and diameters smaller than 10 nm (fig. 1(d)).

Figure 2 shows the ferroelectric and piezoelectric behavior of the PZN-4.5PT single crystals. Figure 2(a) and fig. 2(b) represent the P-E behavior hysteresis of, respectively, the undoped and Mn-doped PZN-4.5PT single crystals. E_c values are slightly the same around 430 V/mm. P_s and P_r decreased slightly (respectively from 0.31 to 0.28 C/m² and from 0.25 to 0.22 C/m²) with the doping. This effect can be explained by the fact that once the

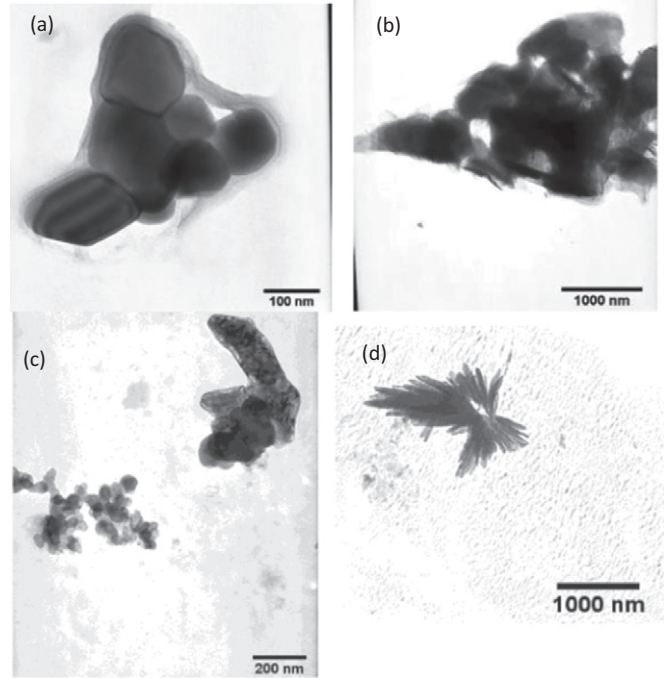


Fig. 1: TEM micrographs for ((a) and (b)) undoped PZN-4.5PT, ((c) and (d)) 1% Mn-doped PZN-4.5PT nanoparticles.

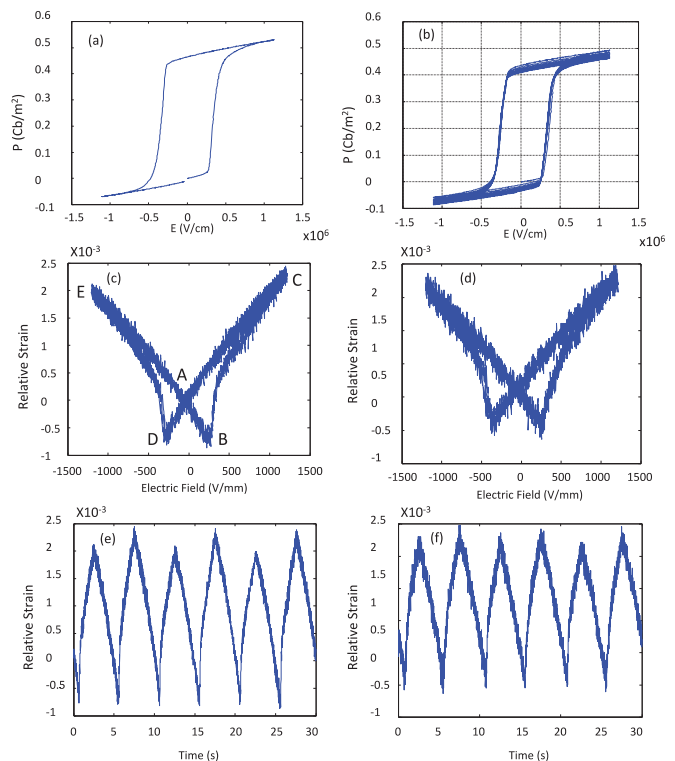


Fig. 2: Hysteresis loops and relative strain of ((a), (c) and (e)) undoped PZN-4.5PT, ((b), (d) and (f)) 1% Mn-doped PZN-4.5PT single crystals.

blocked dipoles were released by a relatively high field they struggled to return to their initial state when the field vanished.

The acceptor dopants such as manganese are known to increase the values of coercive fields and stabilize the dipolar domain distribution within the material. The commonest explanation is linked to the existence of mobile oxygen vacancies that appear under stress and block the movement of domain walls making it more difficult to reverse the polarization and promoting the stability of domains induced by the polarization [15]. Figure 2(c) and fig. 2(d) show butterfly-shaped strain-electric field (S - E) curves. The initial loading cycle started at the point (0, 0). There was no strain response until the electric field reached the coercive field and the material switched to the polarized state. At point A , the material had positive remnant polarization and remnant strain. When a negative electric field was applied, the ions in the crystal structure developed a force that moved them toward a cubic state. When the coercive field was reached at point D , the field value was equal to $-E_c$, the polarization direction began to switch. After the polarization had switched to the direction of the applied electric field, the latter acted to stretch the unit cell, giving a positive strain at point E .

When the electric field was subsequently reduced to zero, the remnant strain coincided with that at point A but the remnant polarization was negative. Thus, as a positive electric field was applied to the negatively polarized material, the ions in the crystal structure again developed a force that moved them toward a cubic state. The coercive field was reached at point B , and the polarization had completely switched direction again at point C . The electric field was reduced to zero and the material returned to point A with positive remnant polarization and remnant strain [16]. Mn doping decreased the relative strain maximum value from 0.25% ($2.5 \cdot 10^{-3}$) for the undoped crystals to a maximum of 0.20% ($2 \cdot 10^{-3}$) for their doped counterparts (fig. 2(e) and fig. 2(f)). These results confirmed the hardness effect of Mn-doping on the characteristics of PZN-PT single crystals.

Magnetic properties of bulks and nanopowders were investigated by measuring field dependence magnetization $M(H)$ at room temperature.

Figure 3 shows the size dependence of PZN4.5PT nanopowders. It is clear from these curves that the magnetic behavior in PZN-4.5PT is related to the size of the crystals and would appear only at the nanoscale level (*i.e.*, in form of powder) and could not be found in the bulk single crystals (which are paramagnetic, fig. 4(a)). There exists an optimized sizes range between 45 to 63 μm for which we have the highest value of the magnetization.

Indeed, due to a high surface-to-volume ratio of atoms in micro- or nanoparticles, a small amount of defects (in the form of cationic or anionic vacancies; formed due to a non stoichiometric ratios between anions and cations in binary semiconductors) is sufficient to show fascinating magnetic properties even when their bulk counterpart

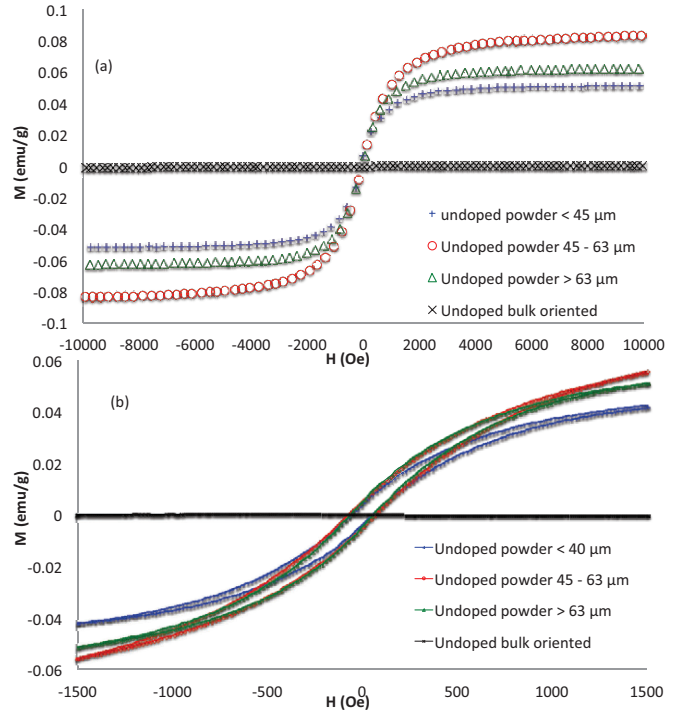


Fig. 3: Size dependence and ferromagnetism nanosize evidence in PZN-4.5PT crystals.

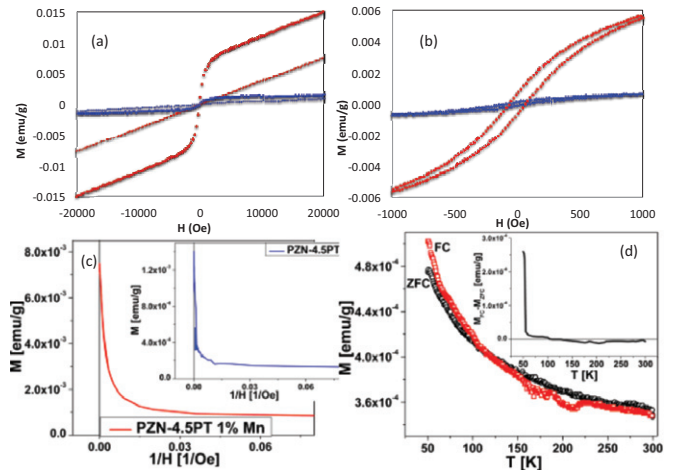


Fig. 4: (a) M - H curves for undoped (o) and 1% Mn-doped PZN-4.5PT powders (o), undoped bulk (---) and doped bulk (---) at high fields. (b) M - H curves at low fields for undoped (o) and 1% Mn-doped PZN-4.5PT (o). (c) M vs. $1/H$ plot. (d) M - T curves at 1000 Oe for 1% Mn-doped PZN-4.5PT nanoparticles; black: ZFC; red: FC.

is non-magnetic [17] (fig. 4). One should recall that in all titanates, entropy requires that there are some oxygen vacancies. Ti^{4+} ions near such vacancies convert to Ti^{3+} , which are magnetic. Therefore, titanates, especially in regions near domain walls (which trap oxygen vacancies) may exhibit unexpected magnetoelectric effects in substances such as SrTiO_3 (PbTiO_3 in our case) that nominally lack magnetic ions [18]. The mechanism

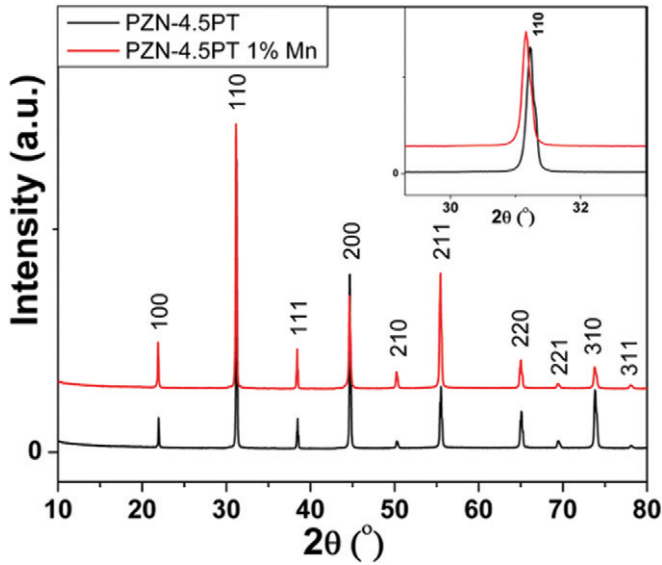


Fig. 5: XRD spectra for PZN-4.5PT and 1% Mn-doped PZN-4.5PT nanopowders after magnetic measurements.

that led to a ferromagnetic behavior being induced in the Ti ions would be T-center exchange (TCE) interactions of $\text{Ti}^{3+}\text{-VO}^{2-}\text{-Ti}^{3+}$ groups (VO^{2-} is oxygen vacancy). Remnant magnetization (M_r) and coercivity (H_c) were measured at low field (fig. 4(b)) and were found equal respectively to 2×10^{-4} emu/g and 63 Oe for undoped and, 7×10^{-4} emu/g and 66 Oe for Mn-doped PZN-4.5PT indicating that the PZN-4.5PT nanoparticles possessed a weak ferromagnetic behavior. The values of the saturated magnetization (M_s) were determined by extrapolating $1/H$ to zero field in the M vs. $1/H$ plot based on high field data (fig. 4(c)). M_s was found equal to 1.0×10^{-3} and 7.5×10^{-3} emu \cdot g $^{-1}$ for the non-uniform undoped and Mn-doped powders. These values are similar to those found in BiFeO_3 ($\approx 4 \times 10^{-2}$ emu \cdot g $^{-1}$) [19]. The presence of an unsaturated hysteresis loop and small remnant magnetization for Mn-doped particles (fig. 4(b)) indicated the canting of the antiferromagnetic spin structure due to size mismatch and/or a ferromagnetic spin structure caused by a different magnetic nature of the substituted Mn [20] as compared to that of the Ti^{3+} ions. The increase in magnetization would be due to the presence of magnetic Mn^{2+} ions that could enhance ferromagnetic properties as well as oxygen vacancies. Mn doping and the reduction of the particle size provided an increased number of $\text{Ti}^{3+}\text{-VO}^{2-}\text{-Ti}^{3+}$ groups (as explained in the previous paragraph), which improved the ferromagnetic behavior. Oxygen vacancies (VO^{2-}) were easily created in the nanocrystals during the doping which significantly promoted the formation of the $\text{Ti}^{3+}\text{-VO}^{2-}\text{-Ti}^{3+}$ groups and increased T-center exchange (TCE) interactions, leading to enhanced room-temperature ferromagnetism. These results are in agreement with Bahoosh *et al.* [21] who have shown that the observed ferromagnetic properties in BaTiO_3 - or PbTiO_3 -nanoparticles at room temperature

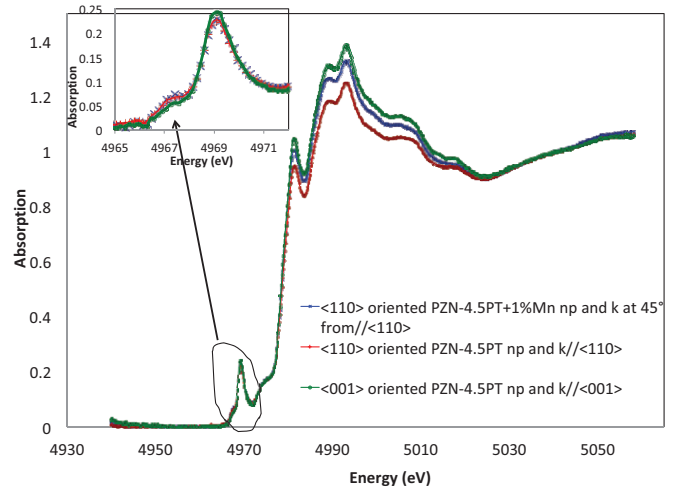


Fig. 6: Ti K-edge Xanes absorption of $\langle 001 \rangle$ and $\langle 110 \rangle$ oriented PZN-4.5PT single crystals using a synchrotron lightsource.

could be originated due to the oxygen vacancies at the surface and to the appearance of a different valence state composed of Ti^{3+} or Ti^{2+} . As a result one observes multiferroic properties of the NP. Whereas the polarization decreases with decreasing particle size, the magnetization increases below a critical particle size N_c that is of the order of 1–8 Å.

This critical particle size should be increased by an external magnetic field.

The field-cooled (FC) and zero-field-cooled (ZFC) magnetization measurements were performed from 50 to 295 K with 1000-Oe applied magnetic fields (fig. 4(d)) for the Mn-doped particles. It can be seen that at temperatures below 221 K, $M(T)$ begins to deviate from linear dependence. The Néel temperature is determined to be $T_N = 221$ K. Such magnetic anomaly was found when antiferromagnetic correlations compete with ferromagnetic interactions. The temperature dependence of the difference magnetization $\Delta M = M_{FC} - M_{ZFC}$ is plotted in fig. 4(d). ΔM shows negative values above 121 K. This unusual feature was related to magnetostriction [22–24]. Our magnetization values were close to those found in BiFeO_3 multiferroic materials [19] and demonstrated that PZN-4.5PT nanoparticles can be considered as multiferroics with excellent properties taking into account their ferroelectric and ferroelastic characteristics.

We performed XRD measurements to reveal the phase composition (fig. 5). The XRD spectra show similar patterns for both samples with characteristic peaks of PZN-4.5PT.

No peaks corresponding to other phases were observed in XRD spectra before and after magnetic measurements indicating pure PZN-4.5PT phase. More generally, it is well known from the literature that mechanical grinding and milling producing more defects in that way treated materials. It is suggested for some defect-rich regions, such as the surface, interface, and grain boundary

(fig. 1). The importance of disordered interfaces and intergranular regions, vacancies, lattice or bond defects are suggested for driving high-temperature ferromagnetic-like behavior [25–27]. It has been also concluded that the proper combination of interpenetrating crystalline and amorphous phases is the most probable condition for the existence of ferromagnetism in pure ZnO [28]. Based on these results we can conclude that grain boundaries, size of the particles and the lattice or bond defects control the ferromagnetic-like properties of the PZN-4.5PT nanoparticles.

Investigations were conducted to determine the different Ti ions present in the crystals. The energies of the Ti^{3+} and nominally Ti^{4+} samples are compared by Waychunas [29]. The mean $1s$ to $3d$ energy for the two Ti^{3+} samples is 4967.5(1)eV, and for the Ti^{4+} samples is 4969.1(1)eV, a shift of 1.6eV. In fig. 6, the Ti K -edge Xanes absorption of $\langle 001 \rangle$ and $\langle 110 \rangle$ oriented PZN-4.5PT single crystals using a synchrotron lightsource indicates the presence of mixed Ti^{3+} and Ti^{4+} ions at the pre-edge position (from 4963–4973eV). The presence of Mn^{2+} and Mn^{3+} ions in the doped crystals may increase the oxygen vacancies. The transformation of Ti^{4+} ions to magnetic Ti^{3+} explain why doping could increase the ferromagnetism of the nanoparticles. It is only at 4967.05eV that the value of Ti ions for Mn-doped crystals is higher than the other crystals (fig. 6). This indicates the presence of Ti^{3+} ions at this position as suggested by [27]. The presence of more Ti^{3+} ions in Mn-doped crystals confirms the hypothesis that oxygen vacancies (VO) would facilitate the transformation of Ti^{4+} to Ti^{3+} ions.

Conclusion. – In this study we have shown that PZN-4.5PT shows excellent magnetic properties when reduced into nanopowder form. The magnetic behavior of undoped and Mn-doped PZN-4.5PT is related to sizes and would appear only at the nanoscale level. Remnant magnetization (M_r) and coercivity (H_c) were measured at low field indicating that the PZN-4.5PT nanoparticles possessed a weak ferromagnetic behavior.

The magnetization values demonstrated that PZN-4.5PT nanoparticles could be considered as multiferroic materials with excellent properties taking into account their ferroelectric and ferroelastic characteristics. The use of the PZN-4.5PT as nanoparticles thin layers allows potential applications in electronic devices.

This work is supported by Agence Universitaire de la Francophonie Bureau Afrique de l’Ouest (AUF-BAO) and LAAAMP joint Project of AflS, ICTP and IUCr.

REFERENCES

- [1] BENEDEK N. A., MULDER A. T. and FENNIE C. J., *J. Solid State Chem.*, **195** (2012) 11.
- [2] PENG D., WANG X., XU C., YAO X., LIN J. and SUN T., *J. Am. Ceram. Soc.*, **96** (2013) 184.
- [3] MATAR S. F., *Progr. Solid State Chem.*, **40** (2012) 31.
- [4] BISHOP A. R., *J. Phys. Chem. Solids*, **65** (2004) 1449.
- [5] ROESKY H. W., HAIDUC I. and HOSMANE N. S., *Chem. Rev.*, **103** (2003) 2579.
- [6] SONG F., SHEN X., LIU M. and XIANG J., *J. Solid State Chem.*, **185** (2012) 31.
- [7] CHENG J.-R., LI N. and CROSS L. E., *J. Appl. Phys.*, **94** (2003) 5153.
- [8] VAN SUCHTELEN J., *Philips Res. Rep.*, **27** (1972) 28.
- [9] BOOMGAARD J. V. D., VAN RUN A. and VAN SUCHTELEN J., *Ferroelectrics*, **14** (1976) 727.
- [10] ZHENG H., WANG J., LOFLAND S. E., MA Z., MOHADDES-ARDABILI L., ZHAO T., SALAMANCA-RIBA L., SHINDE S. R., OGALE S. B., BAI F. *et al.*, *Science*, **303** (2004) 661.
- [11] LEBRUN L., ZHANG S., RANDALL C. A., SHROUT T. R. and GUYOMAR D., *Ceram. Trans.*, **136** (2002) 117.
- [12] BENAYAD A., KOBOR D., LEBRUN L., GUIFFARD B. and GUYOMAR D., *J. Cryst. Growth*, **270** (2004) 137.
- [13] KOBOR D., TINE M., HAJJAJI A., LEBRUN L. and GUYOMAR D., *J. Mod. Phys.*, **3** (2012) 402.
- [14] PRIYA S. and UCHINO K., *J. Appl. Phys.*, **91** (2002) 4515.
- [15] CHEN Y. H., HIROSE S., VIEHLAND D., TAKAHASHI S. and UCHINO K., *Jpn. J. Appl. Phys.*, **39** (2000) 4843.
- [16] LYNCH C. S., *Acta Mater.*, **44** (1996) 4137.
- [17] SUNDARESAN A. and RAO C. N. R., *Nano Today*, **4** (2009) 96.
- [18] SCOTT J. F., *npj Comput. Mater.*, **1** (2015) 15006.
- [19] SURESH P. and SRINATH S., *J. Alloys Compd.*, **649** (2015) 843.
- [20] KUMAR P. and KAR M., *Phys. B: Condens. Matter.*, **448** (2014) 90.
- [21] BAHOSH S. G., TRIMPER S. and WESSELINOWA J. M., *Phys. Status Solidi RRL*, **5** (2011) 382.
- [22] ZHAO B. C., MA Y. Q., SONG W. H. and SUN Y. P., *Phys. Lett. A.*, **354** (2006) 472.
- [23] TADIC M., MILOSEVIC I., KRALJ S., MBODJI M. and MOTTE L., *J. Phys. Chem. C*, **119** (2015) 13868.
- [24] TADIC M., MILOSEVIC I., KRALJ S., SABOUNGI M. L. and MOTTE L., *Appl. Phys. Lett.*, **106** (2015) 183706.
- [25] COEY J. M. D., *Solid State Sci.*, **7** (2005) 660.
- [26] PENG H., LI J., LI S. S. and XIA J. B., *Phys. Rev. B*, **79** (2009) 092411.
- [27] WANG Y. G., TANG X. G., LIU Q. X., JIANG Y. P. and JIANG L. L., *Nanomaterials*, **7** (2017) 264.
- [28] STRAUMAL B. B. *et al.*, *Beilstein J. Nanotechnol.*, **7** (2016) 1936.
- [29] GLENN WAYCHUNAS A., *Am. Miner.*, **72** (1987) 89.